Supporting Information

ZnS Spheres Wrapped by Ultrathin Wrinkled Carbon film as Multifunctional Interlayer for Long-life Li-S Batteries

Jin-Lin Yang[a,b], Shi-Xi Zhao[a*], Yi-Ming Lu[a,b], Xiang-Tian Zeng[a,b], Wei Lv[a] and Guo-Zhong Cao[c*]

[a] Tsinghua Shenzhen International Graduate School, Tsinghua University, Shenzhen, 518055, China.

[b] School of Materials Science and Engineering, Tsinghua University, Beijing, 100084, China.

[c] Department of Materials Science and Engineering, University of Washington, Seattle, WA 98195, USA.

*Corresponding author: Email: zhaosx@sz.tsinghua.edu.cn (S.X.Zhao); E-mail: gzcao@uw.edu

Supplementary Figures

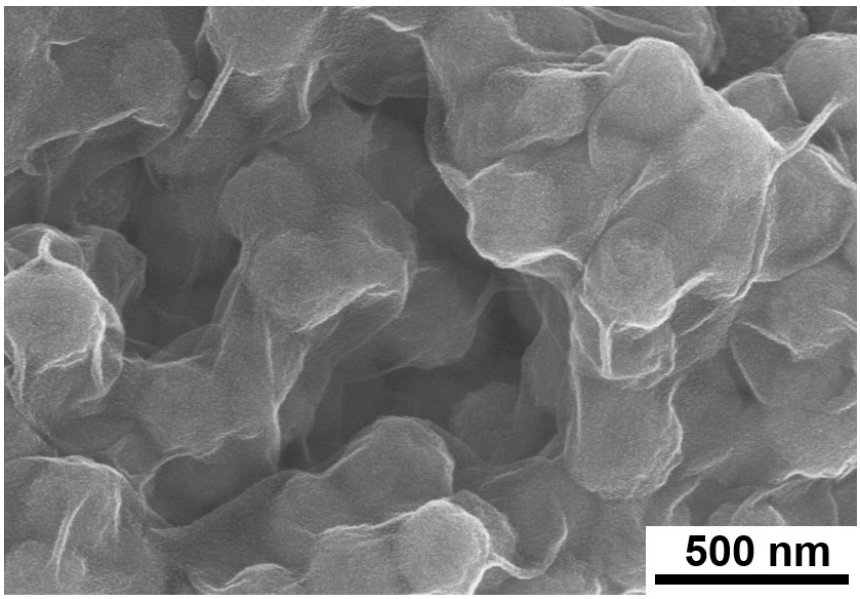

Figure S1. SEM image of ZnS@WCF

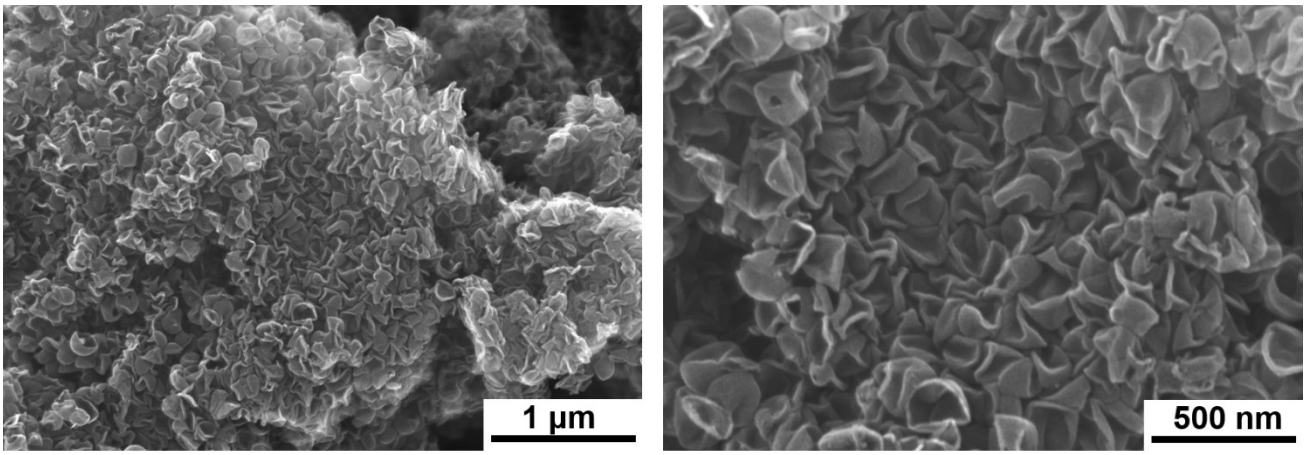

Figure S2. SEM images of pure WCF

Table S1. Synthesis details of ZnS@WCF.

Samples	RF (g/ml)	TPOS (ml)	$NH_3 \cdot H_2O$	Water/ethanol (ml/ml)
A	0.10-0.14	2.5	3	10/70
B	0.05-0.07	2.5	3	10/70
C	0.0125-0.0175	2.5	3	10/70
D	0.025-0.035	5	3	10/70
E	0.025-0.035	1.25	3	10/70
F	0.025-0.035	2.5	3	20/60
G	0.025-0.035	2.5	1.5	10/70
H	0.025-0.035	2.5	6	10/70
I	0.025-0.035	2.5	12	10/70
J	Same to the synthesis process of ZnS@WCF, but TPOS and RF were added simultaneously			
ZnS@WCF	0.025-0.035	2.5	3	10/70

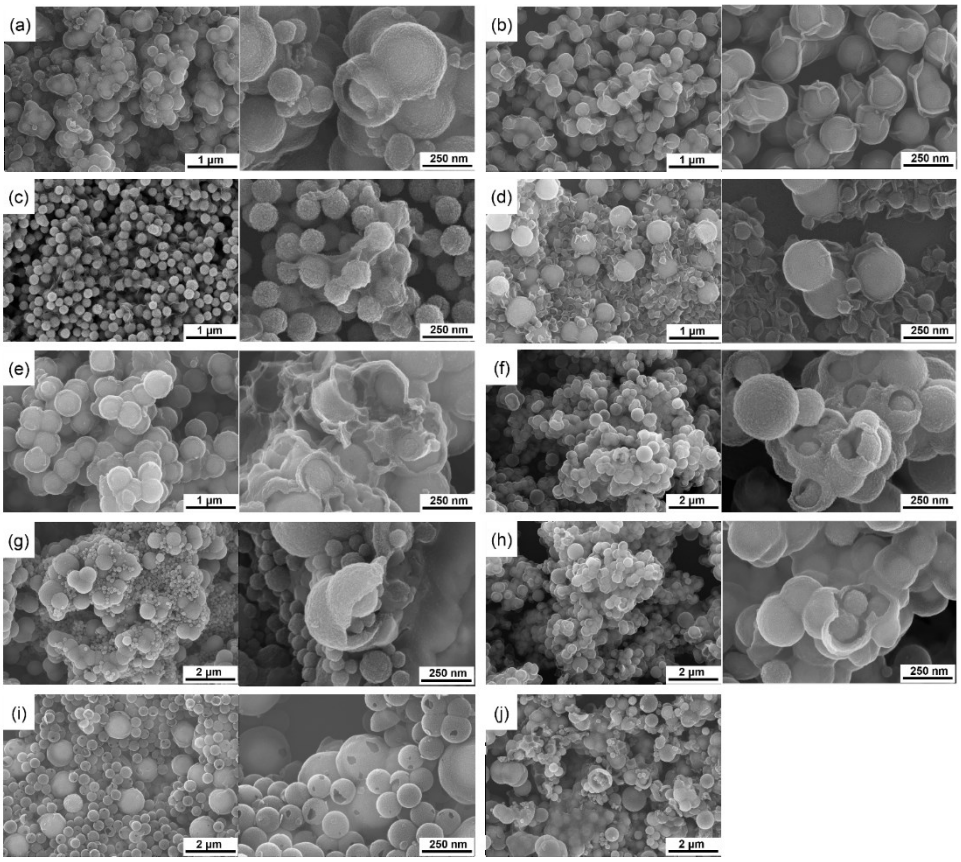

Figure S3. SEM images of different samples fabricated throughout the process mentioned in Table S2. (a)-(j) are corresponded to the sample A-J repectively.

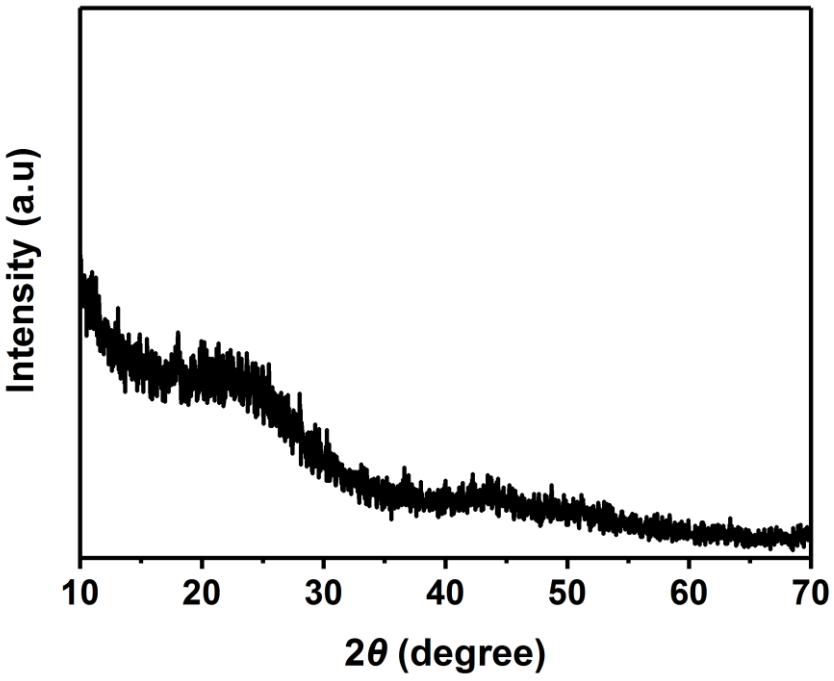

Figure S4. XRD pattern of the pure WCF sample.

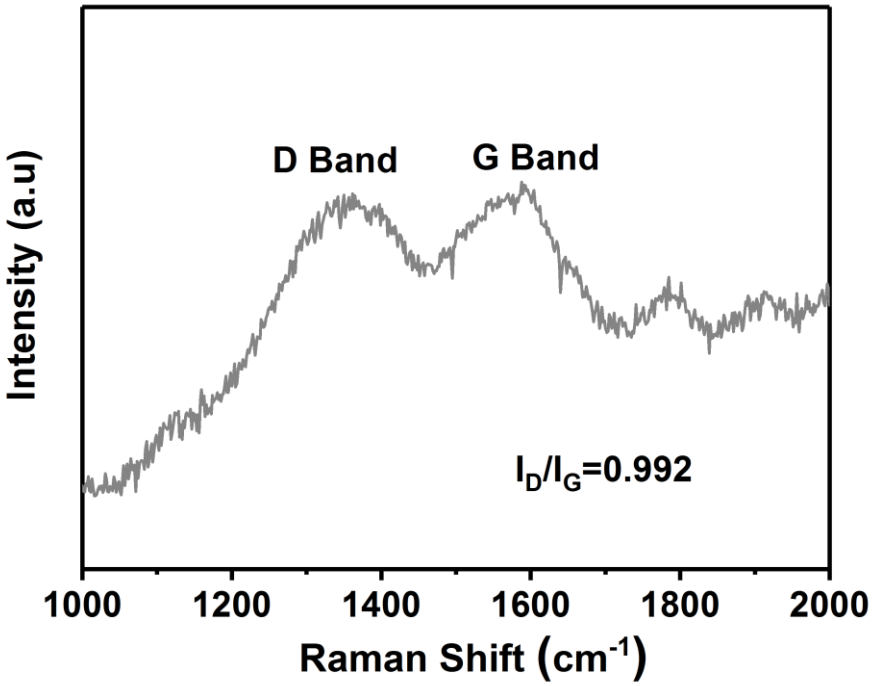

Figure S5. Raman spectra of ZnS@WCF

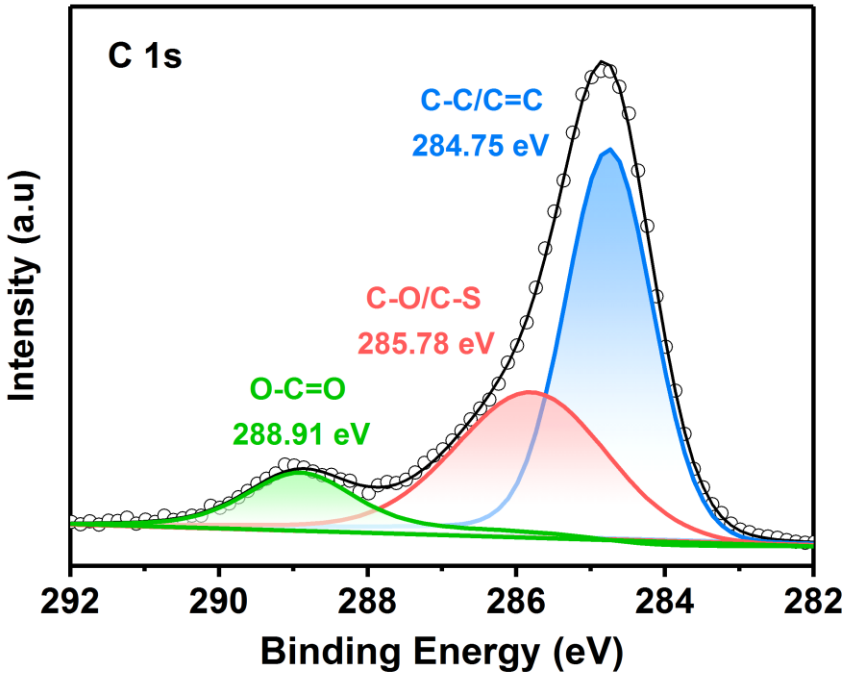

Figure S6. High resolution XPS spectra of C 1s in ZnS@WCF

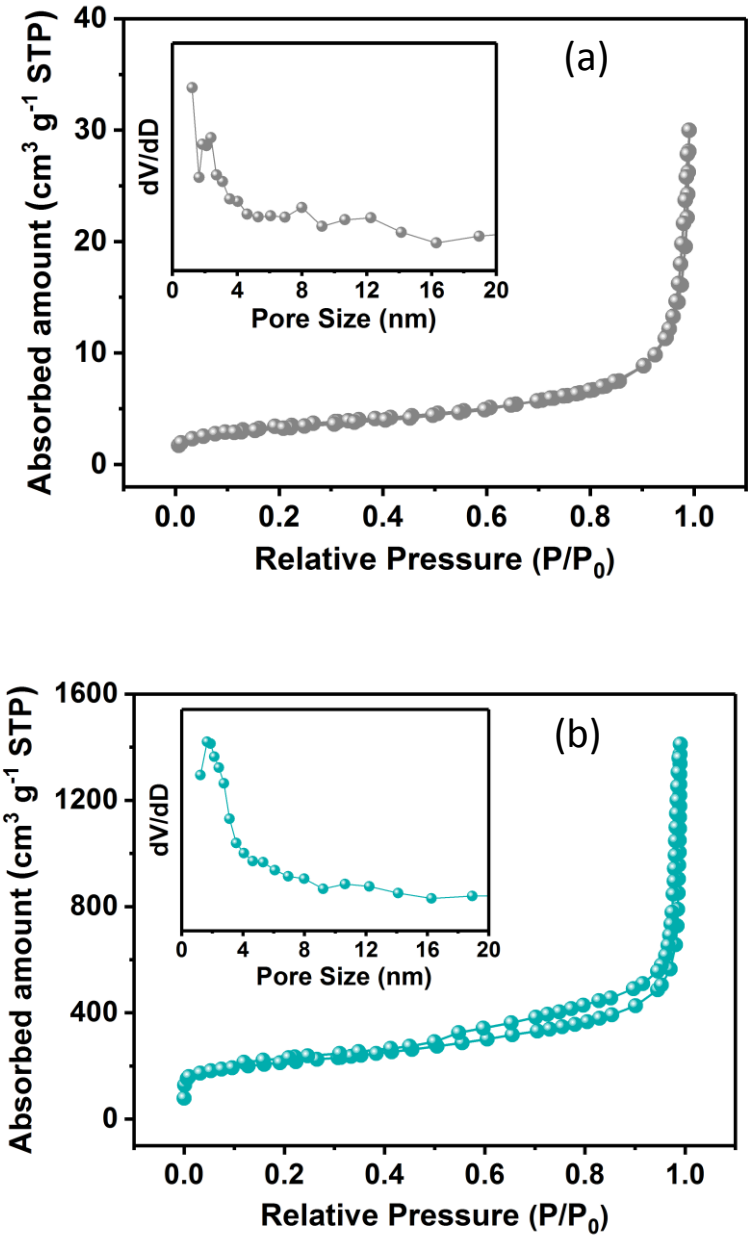

Figure S7. N_2 sorption isotherms and pore distribution of (a) ZnS nanospheres and (b) WCF

Table S2. S_{BET} and V_P values of samples.

Samples	ZnS nanospheres	WCF	ZnS@WCF
S_{BET} ($m^2 \cdot g^{-1}$)	12.532	768.05	446.95
V_P ($m^3 \cdot g^{-1}$)	0.0434	1.943	0.7389
Pore Size (nm)	1.21	1.66	1.64

Theoretical equations of the current-time transients of four classic electrochemical deposition models (2D instantaneous nucleation and 2D progressive nucleation are based on Bewick, Fleischman, and Thirsk models; 3D instantaneous nucleation and 3D progressive nucleation are based on Scharifker–Hills models):[47]

2DI:

$$\frac{i}{i_m} = (\frac{t}{t_m})\{\exp[\frac{t^2 - t_m^2}{2t_m^2}]\} \quad \text{(S1)}$$

2DP:

$$\frac{i}{i_m} = (\frac{t}{t_m})^2\{\exp[\frac{-2(t^3 - t_m^3)}{3t_m^3}]\} \quad \text{(S2)}$$

3DI:

$$\frac{i}{i_m} = (\frac{1.9542}{t/t_m})^{1/2}\{1 - \exp[1.2564(\frac{t}{t_m})]\} \quad \text{(S3)}$$

3DP:

$$\frac{i}{i_m} = (\frac{1.2254}{t/t_m})^{1/2}\{1 - \exp[2.3367(\frac{t}{t_m})^2]\} \quad \text{(S4)}$$

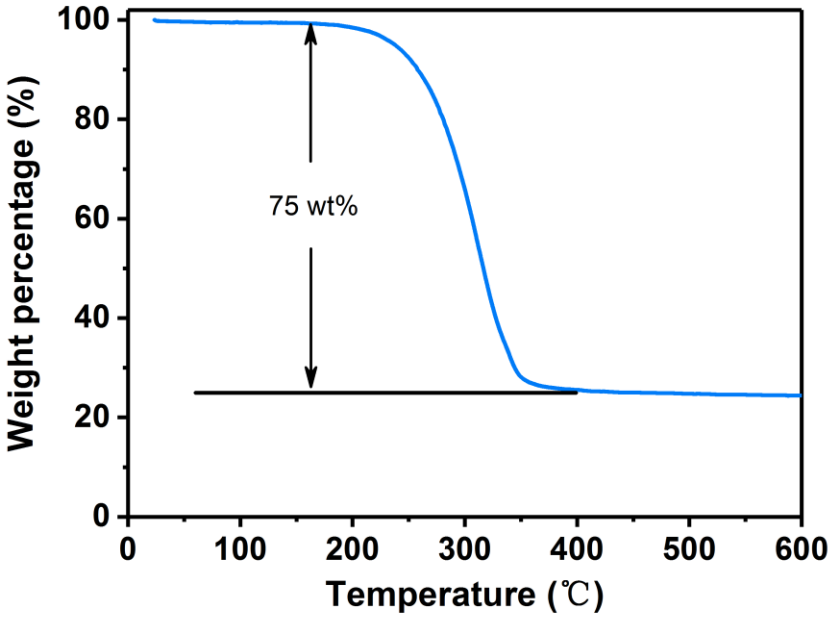

Figure S8. TGA curve of CB/S hybrid under N_2 atmosphere.

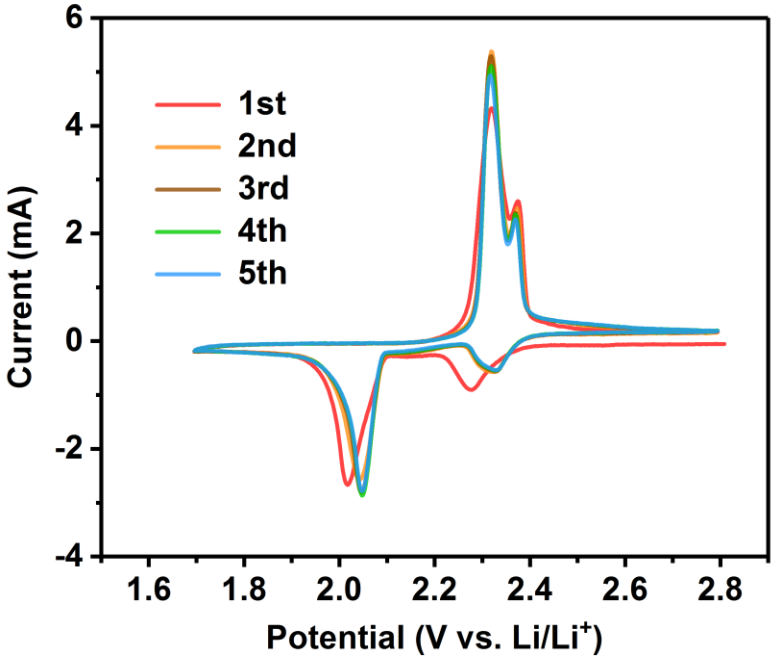

Figure S9. The initial five CV curves of LS-ZnS@WCF at a scan rate of 0.1 $mV \cdot s^{-1}$

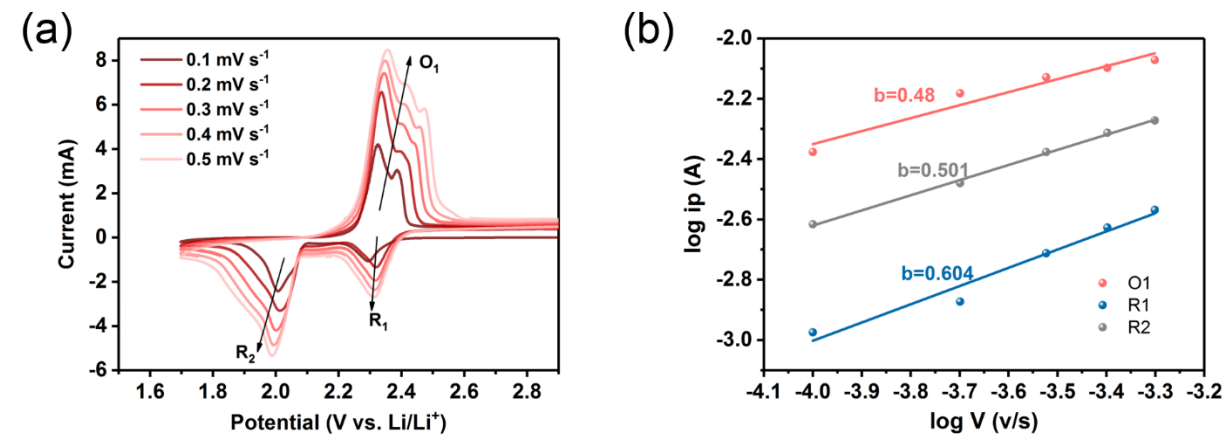

Figure S10. (a) CV curves at different scan rates ranging from 0.1 to 5 mV s^{-1}; (b) The plots of log ip as a function of log *v*.

As we can see from the CV curves, the polarization and the width of current peaks increased with the scan rate. The power law formulas $ip = a \cdot v^b$ and $\log ip = \log a + b \log v$ can be employed for the analysis of the CV data obtained. Ip is the current of the oxidation peak and the reduction peaks (O_1, R_1 and R_2). v represents the scan rate. Two well-defined conditions should be introduced: i) b = 1.0 is representative of surface-capacitive behavior and ii) b = 0.5 suggests a faradaic intercalation process, which is Li^+ diffusion controlled. b is equal to the slope of plots in the right fig. We found that the values of b are in the range of 0.48-0.6, indicating the Li^+ diffusion-controlled process during the electrochemical reaction. [S1,S2]

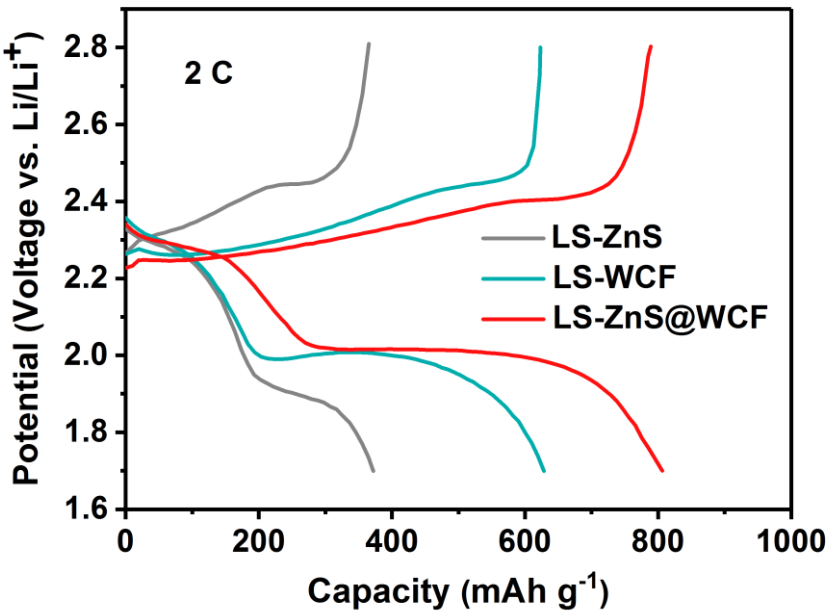

Figure S11. Charge-discharge profiles of L-S cells based on different type of interlayers at 2 C.

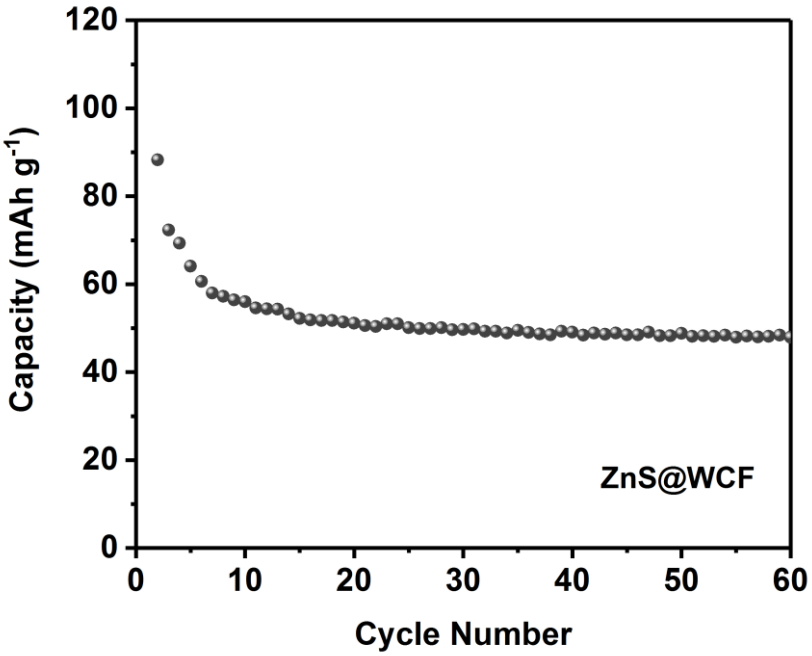

Figure S12. Cycling performance of ZnS@WCF hybrid without the addition of CB/S cathode.

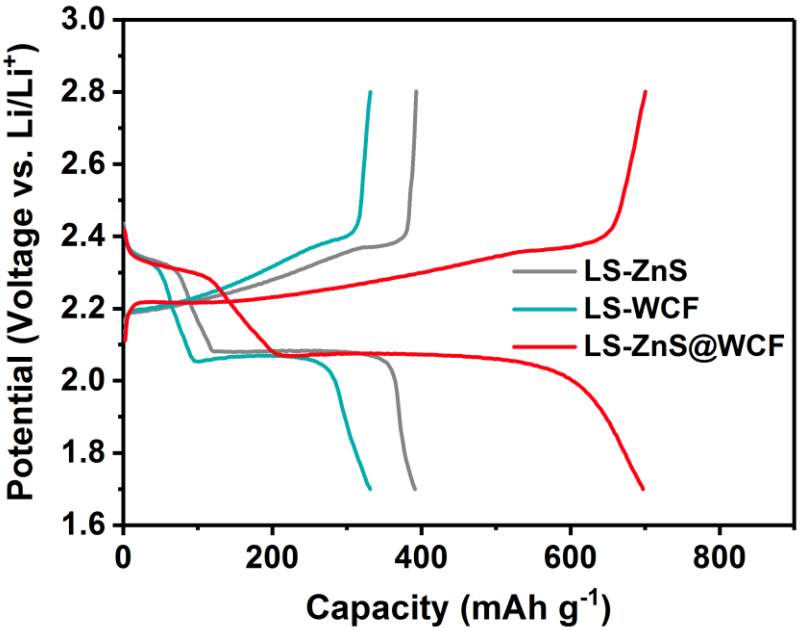

Figure S13. Charge-discharge profiles of L-S cells based on different type of interlayers after 300 cycles at 0.5 C.

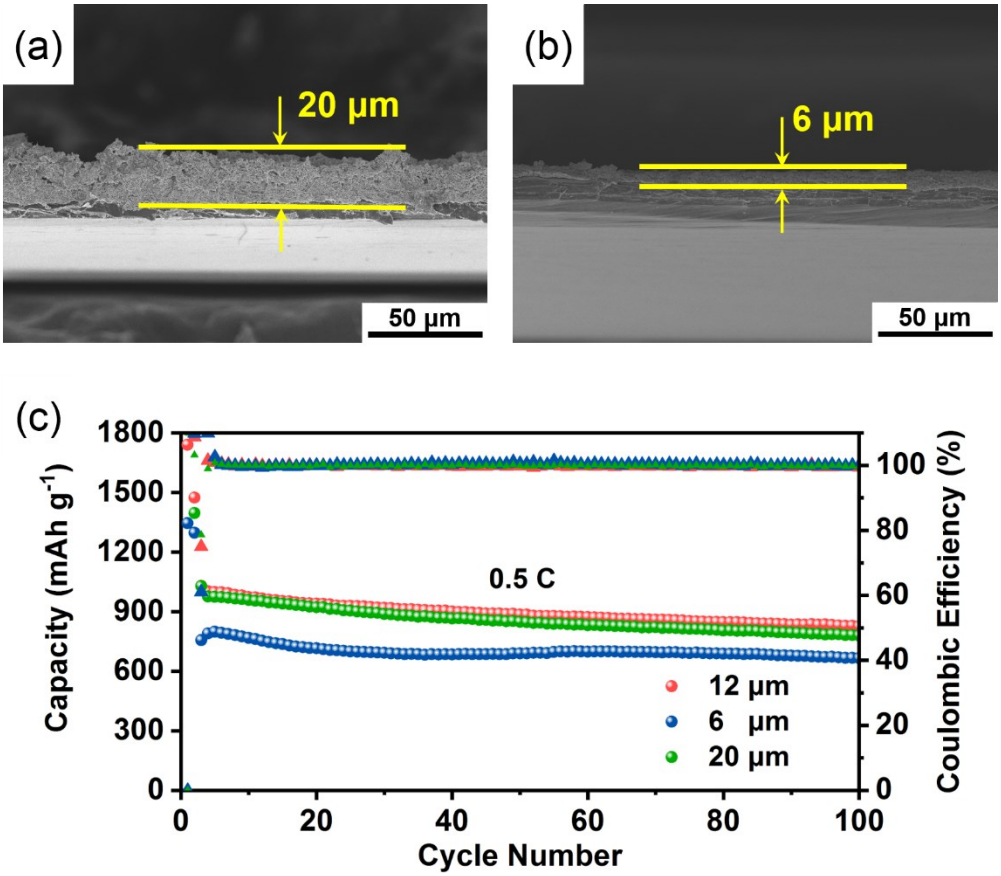

Figure S14. (a),(b) SEM images of ZnS@WCF coated separator with different thickness; (c) Cycling performance of LS-ZnS@WCF based on different interlayer thickness at 0.5 C.

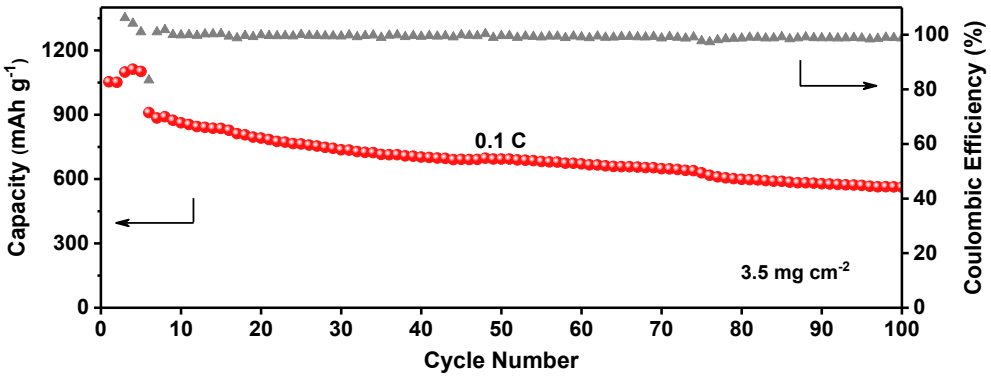

Figure S15. Cycling performance of LS-ZnS@WCF with a high areal sulfur loading of 3.5 mg·cm^{-2} at 0.1 C.

Table S2. Comparison of electrochemical performances of the other hybrid interlayer materials in recent reported literatures.

Materials	Current density	Cycle number	Capacity decay rate (%)	Rate performance	Ref
SnO_2-rGO	1 C	200	0.15	734 mAh g^{-1}, 2C	17
Laponite-CB	0.2 C	500	0.06	758 mAh g^{-1}, 2C	[S3]
MoO_3-CNTs	1 C	400	0.12	764 mAh g^{-1}, 2C	[S4]
Co/mSiO_2-NCNTs	1 C	250	0.09	552 mAh g^{-1}, 5C	[S5]
HEMO-KB	0.5 C	600	0.077	634 mAh g^{-1}, 1C	[S6]
PDA-rGO	0.1	100	0.28	460 mAh g^{-1}, 2C	[S7]
ZnS@WCF	1 C	600	0.045	807 mAh g^{-1}, 2C	This work

References

[1] J. Wang, J. Polleux, J. Lim and B. Dunn, J. Phys. Chem. C, 2007, 111, 14925–14931.

[2] X. H. Rui, N. Yesibolati, S. R. Li, C. C. Yuan and C. H. Chen, Solid State Ionics, 2011, 187, 58–63.

[3] Y. Yang, J. Zhang, Adv. Energy Mater. 8 (2018) 1801778.

[4] L. Luo, X. Qin, J. Wu, G. Liang, Q. Li, M. Liu, F. Kang, G. Chen, B. Li, J. Mater. Chem. A. 6 (2018) 8612-8619.

[5] D. Fang, Y. Wang, X. Liu, J. Yu, C. Qian, S. Chen, X. Wang, S. Zhang, ACS Nano 13 (2019) 1563-1573.

[6] Y. Zheng, Y. Yi, M. Fan, H. Liu, X. Li, R. Zhang, M. Li, Z.-A. Qiao, Energy Storage Mater. (2019).

[7] F. Wu, S. Zhao, J. Li, Y. Lu, Y. Su, L. Chen, L. Bao, J. Yao, X. Liu, ACS Appl. Mater. Interfaces 11 (2019) 12544-12553.